

Available online at www.sciencedirect.com

ScienceDirect

journal homepage: www.jfda-online.com

Original Article

In vitro and in vivo assessment of delivery of hydrophobic molecules and plasmid DNAs with PEO–PPO–PEO polymeric micelles on cornea



Feichin Hsiao^a, Po-Yang Huang^a, Takao Aoyagi^b, Shwu-Fen Chang^c, Jiahorn Liaw^{a,*}

^a School of Pharmacy, College of Pharmacy, Taipei Medical University, 250 Wu-Hsing Street, Taipei 11031, Taiwan

^b Department of Materials and Applied Chemistry, College of Science and Technology, Nihon University, Chiyoda, Tokyo 101-8308, Japan

^c Graduate Institute of Medical Sciences, College of Medicine, Taipei Medical University, 250 Wu-Hsing Street, Taipei 11031, Taiwan

ARTICLE INFO

Article history:

Received 11 July 2017

Received in revised form

29 August 2017

Accepted 17 September 2017

Available online 10 November 2017

Keywords:

Cornea

Eye drops

Polymeric micelles

Stability

ABSTRACT

The stability and bio-distribution of genes or drug complexes with poly(ethylene oxide)-poly(propylene oxide)-poly(ethylene oxide) (PEO–PPO–PEO, Pluronic F-68) polymeric micelles (PM) are essential for an effective nanosized PM delivery system. We used Förster resonance energy transfer (FRET) pairs with PM and measured the FRET ratio to assess the stability of PM *in vitro* and *in vivo* on the cornea. The FRET ratio reached a plateau at 0.8 with 3% PM. Differential scanning calorimetry measurement confirmed the complex formation of FRET pairs with PM. Confocal imaging with the fluorophores fluorescein isothiocyanate isomer I (FITC) and rhodamine B base (RhB) also showed the occurrence of FRET pairs *in vitro*. The fluorophores were mixed with 3% PM solution or the FITC-labeled PEO–PPO–PEO polymers (FITC-P) were mixed with RhB-labeled plasmids (RhB–DNA). In addition, the *in vitro* corneal permeation of FRET pair complexes with PM reached a 0.8 FRET ratio. One hour after eye drop administration, FRET pairs colocalized in the cytoplasm, and surrounded and entered the nuclei of cells in the cornea, and the polymers were located in the corneal epithelial layers, as detected through anti-PEG immunohistochemistry. Furthermore, fluorescence colocalization in the cytoplasm and cell nucleus of the corneal epithelium was confirmed in tissues where RhB or RhB–DNA complexed with FITC-P was found to accumulate. We demonstrate that at a concentration of 3%, PM can encapsulate FRET pairs or RhB–DNA and retain their integrity within the cornea 1 h after administration, suggesting the feasibility and stability of PEO–PPO–PEO polymers as a vehicle for drug delivery.

Copyright © 2017, Food and Drug Administration, Taiwan. Published by Elsevier Taiwan LLC. This is an open access article under the CC BY-NC-ND license (<http://creativecommons.org/licenses/by-nc-nd/4.0/>).

* Corresponding author. Fax: +886 2 23779873.

E-mail address: jhorn@tmu.edu.tw (J. Liaw).

<https://doi.org/10.1016/j.jfda.2017.09.002>

1021-9498/Copyright © 2017, Food and Drug Administration, Taiwan. Published by Elsevier Taiwan LLC. This is an open access article under the CC BY-NC-ND license (<http://creativecommons.org/licenses/by-nc-nd/4.0/>).

1. Introduction

Biocompatible poly(ethylene oxide)-poly(propylene oxide)-poly(ethylene oxide), known as PEO–PPO–PEO triblock copolymers, have drawn increasing attention as a pharmaceutical application because of the hydrophilic PEO ends that provide a steric barrier against opsonization [1,2]. In addition, the self-assembly of the hydrophobic core of PEO–PPO–PEO block copolymers provides a microenvironment for water-insoluble molecules and is believed to facilitate solubility in polymeric micelles (PM) [1]. Thus, PEO–PPO–PEO PM have been used as carriers for the IV injection of the anti-inflammatory agent (methylprednisolone) [3] and the antineoplastic agent (doxorubicin) [4], as well as oral non-viral gene delivery [5], intramuscular sustained release formulations [6], and transdermal patch or inhalation applications [7,8].

Stability is a predominant factor that affects the efficiency of PM carrier systems. In contrast to relatively stable nanocarriers with solid-like cores, it remains unclear whether PM dissociates to free polymer chains and attains dynamic equilibrium after extreme dilution. Because the concentration of PM carriers in a biological system is likely to decline to a level below the critical micelle concentration (CMC), the minimum concentration at which amphiphilic polymers assemble to form PM, real-time monitoring of the micelle status and drug retention within the PM is necessary for successful delivery [9]. Förster resonance energy transfer (FRET) between two fluorescent probes is used to determine when two molecules are close to one another on a molecular scale ($<80 \text{ \AA}$), as well as whether both molecules are moving relative to each other [10]. The FRET ratio is generally used to determine whether two fluorophores are within a certain distance of each other. Thus, FRET has been extensively used as a spectroscopic ruler for nanosized particles to determine fluorophore proximity and the release of hydrophobic molecules from carriers [11].

Visual impairment caused by trauma, macular degeneration, diabetic retinopathy, or glaucoma, is the leading cause of blindness worldwide. According to the World Health Organization, an approximately 39 million people out of 285 million cases of visual impairment in 2010 were cases of blindness [12]. Delivery of anti-inflammatory [13], antiglaucoma drugs, or gene therapy to the eyes provides additional options for ophthalmic treatments. Topical instillation of ophthalmic drops is the most common method of administering drugs to treat ocular disease. PEO–PPO–PEO has been approved by the United States Food and Drug Administration for use in ophthalmic pharmaceuticals [14]. However, drug delivery to the eyes has remained a challenging task, due to the difficulties associated with absorption of topical drugs in the tightly structured corneal epithelium and the anteriorly directed aqueous humor bulk flow. The other major barrier to the development of drugs composed of small molecules or genes is the instability of the process. Such instability can lead to immunogenicity and loss of activity, such as genes being further destabilized by nucleases [15].

Although PM has been used as topical ocular vehicles to facilitate delivery of therapeutic genes to the cornea [16–18], it is critical to illustrate the delivery pathway of PM to determine whether the integrity and stability of the PM complex and its

cargo remain intact [19,20]. Obstacles that PM could encounter after penetrating the cornea includes tear flow which has a high turn-over rate, and the stratified multi-layered corneal epithelium which has high resistance barrier to foreign substances [21]. Therefore, we applied a fluorogenic-based approach with two hydrophobic fluorophore FRET dyes: fluorescein isothiocyanate isomer I (FITC) and rhodamine B base (RhB). We took advantage of the transparent characteristic of the cornea to investigate the stability and biodistribution of PM and its cargo, by using free hydrophobic fluorophore molecules, fluorophore-labeled DNA (RhB–DNA), or PEO–PPO–PEO block copolymers.

2. Materials and methods

2.1. Materials

PEO–PPO–PEO copolymers (PEO/PPO/PEO = 76/30/76, Pluronic F-68), with an average molecular mass of 8400 Da, were purchased from BASF (Ludwigshafen, Germany). FITC and RhB were obtained from Sigma–Aldrich (St. Louis, MO, USA). All other chemicals were of analytical grade and used as received. Chemical conjugation and purification of the PEO–PPO–PEO with FITC (FITC–P) moiety at the chain end were performed by following the procedures from our previous studies [22].

2.2. Animals

Six- to eight-week-old male nude mice (BALB/c-nu), as the selection of the animal model of the previous gene delivery experiment [17], were obtained from the National Laboratory Animal Breeding and Research Center (Taipei, Taiwan). The mice were maintained under specific pathogen-free conditions and housed under standard conditions with a 12-h light–dark cycle. The protocols on the use of animals were approved by the Laboratory Animal Research Committee of Taipei Medical University.

2.3. Plasmid DNA labeling

A plasmid, pCMV-bcl-xL-eGFP (5.7 kb), was constructed according to previous protocols [18] and amplified in the *Escherichia coli* DH5 α strain. The plasmid was purified using equilibrium centrifugation with a CsCl–EtBr gradient. RhB was covalently attached to 100 μg of pCMV–bcl-xL–eGFP DNA using a Label IT Nucleic Acid Labeling Kit (Mirus Corp., Madison, WI, USA). Label IT Reagent (100 μl) in the buffers was mixed with DNA, and the mixture was incubated at 37 $^{\circ}\text{C}$ for 2 h in the dark. Unincorporated dye was removed, and labeled DNA was purified using ethanol precipitation. Concentrations of DNA were measured through UV absorption. Labeling efficiencies were estimated to be one label for every 60 base pairs, by using a spectrophotometric assay and following a protocol provided by the manufacturer.

2.4. Preparation of PEO–PPO–PEO PM

All concentrations of polymeric solution were prepared on a weight percentage basis according to previous protocols

[16]. Pyrene fluorescent dyes, used as probes for determining the CMC, and 180 μM FITC or various concentrations of RhB were mixed with PEO–PPO–PEO PM in a vial at 25 °C. Using similar procedures, 3 μM RhB or RhB–DNA (80 ng/ μl) with 3% FITC–P solutions was also prepared. Then, 80 ng/ μl RhB–DNA was added to 3% FITC–P solutions with gentle mixing at 25 °C.

2.5. Transmission electron microscopy

PM morphology was evaluated from Transmission electron microscopy (TEM) images using a Hitachi HT7700 operating at an acceleration voltage of 75 kV. The sample was stained with uranium acetate and deposited on a carbon–Formvar-coated nickel grid (200 mesh) (TAAB Laboratories Equipment Ltd., Berkshire, UK).

2.6. Atomic force microscopy

PM was prepared for imaging by placing a dispersion (3 μl) of each sample onto freshly cleaved mica, and then the surface was air dried. Atomic force microscopy (AFM) (diCP-II; Digital Instruments/Veeco Metrology Group, Santa Barbara, CA) was operated at 25 °C. Scanning was performed in tapping mode using cantilevers with a rectangular 3.4 \times 1.6 \times 0.4 mm silicon chip (resonant frequency = 265–400 kHz, force constant = 20–75 N m^{-1} , tip radius < 10 nm; MikroMasch, Estonia). The constant force mode was used with a resonant scan frequency of 375 kHz, and the images were subsequently processed using Proscan software (V 1.8.00, Digital Instruments/Veeco Metrology Group, Santa Barbara, CA). All images were collected within 1 \times 1 μm^2 areas.

2.7. Zeta-potential measurements

The zeta-potential was assessed by dynamic light scattering (DLS) using a Zetasizer NanoZS (Malvern Instruments, Worcestershire, UK). Samples were freshly prepared and measured at 25 °C with a He–Ne laser at a wavelength of 633 nm, and phase analysis light scattering (PALS) was performed at angles of 13° and 173°. The results were average after triplicate measurements.

2.8. The critical micelle concentration

The formation of PM was confirmed using a fluorescence probe pyrene partition protocol [22]. The partitioning of pyrene into PM can be determined using the ratio peak I_1/I_3 of the pyrene spectrum as described in our previous studies [16,22]. The fluorescence emission spectrum of pyrene in the PEO–PPO–PEO polymer solutions was measured from 350 to 450 nm with a fixed excitation wavelength of 339 nm. The concentration of PEO–PPO–PEO polymer solutions measured varied from 0.001 to 10% (w/w) with a constant pyrene concentration of 6×10^{-7} M. The various concentrations of PEO–PPO–PEO polymers and spectral data were acquired using a Hitachi F4500 fluorescence spectrophotometer. All fluorescence experiments were conducted at 25 °C.

2.9. FRET measurements

Fluorescence measurements were performed using a Variskan Flash Multimode Reader (Thermo Fisher Scientific Inc., Waltham, MA, USA). To verify the occurrence of FRET between FITC and RhB, 2 μl of a series of concentrations of paired fluorophores in DMSO was mixed with 100 μl of 3% or different concentrations of PM solutions. The FITC and RhB complexes with PM solutions were measured at an excitation wavelength of 490 nm and with an emission scan from 505 to 650 nm. The FRET ratio was calculated as $I_{576}/(I_{520} + I_{576})$ as described in a previous study [23], where I_{520} and I_{576} are the fluorescence emission intensities of the donor (FITC) and the acceptor (RhB) after excitation at 490 nm, respectively.

2.10. Differential scanning calorimetry

To understand the interaction between FRET pairs and PM, a differential scanning calorimetry (DSC) analysis was conducted using a Shimadzu DSC-60 plus (Shimadzu, Tokyo, Japan). After the samples were crimped in aluminum pans and transferred to the DSC cell, they were heated from 30 °C to 450 °C at a rate of 5 °C/min under a nitrogen atmosphere after one cycle.

2.11. Confocal laser scanning microscopy

All images were acquired using a Leica TCS SP5 Confocal Spectral Microscope Imaging System (Leica Microsystems, Wetzlar, Germany). An argon laser was excited at 488 nm and the emission data were collected at 500–550 nm for the donor (FITC) channel and 565–650 nm for the acceptor (RhB) channel. All of the images were captured and processed with Leica Application Suite-Advanced Fluorescence software (Leica LAS AF). The images represented three independent experiments.

2.12. In vitro corneal permeation of FRET pairs

To investigate the permeation of FRET pairs (FITC and RhB) with PM (0.2 ml) through the cornea, a fresh nude mouse cornea was excised immediately after cervical dislocation, according to previous studies [5,7,8,16], and mounted carefully between two compartments of a Franz cell with a rigid clamp. The surfaces of the donor and the receiver of a Franz cell were covered with silicone gel O ring sheets to prevent the leakage. The receiver compartment (3 ml) was filled with glutathione bicarbonate Ringer's (GBR) solution (pH 7.4) which was stirred throughout the permeation study at 37 °C and contacted a 0.025 cm^2 area of the cornea. Samples (0.2 ml) were collected from the receiver compartment at fixed intervals and replaced with an equal volume of previously warmed GBR solution. The FRET pairs with PM were measured at the excitation and emission wavelengths of 490 nm and 576 nm, respectively. The FRET ratio was calculated as $I_{576}/(I_{520} + I_{576})$, as previously mentioned. The experiments were repeated four times.

2.13. Intracorneal distribution

Eye drops (10 μl) were administered to the nude mice. One hour after administration, the mice were sacrificed through

cervical dislocation as in previous studies [16]. The corneal specimens were freshly excised and mounted on glass slides. Samples were immediately imaged without additional tissue processing using confocal laser scanning microscopy. All images were captured and processed as described in Section 2.11.

2.14. Corneal immunostaining

After observation of intracorneal distribution, the freshly excised corneas were fixed in 4% paraformaldehyde at room temperature for 3 h. Sections (5 μm) were placed on glass slides after the tissues were dehydrated and paraffin embedded. Deparaffinized slides were immunostained overnight at 4 $^{\circ}\text{C}$ with the anti-PEG rabbit mAb PEG-B-47 (Abcam, Cambridge, MA, USA). Sections of the cornea were then stained at 25 $^{\circ}\text{C}$ for 1 h with the Alexa Fluor 568-conjugated donkey anti-rabbit IgG H&L (Abcam, Cambridge, MA, USA) secondary antibody and mounted using Vectashield HardSet containing DAPI (Vector Lab, Burlingame, CA, USA).

2.15. Statistical analysis

Statistical analysis of the samples was performed with one-way analysis of variance in combination with Scheffe's post-hoc test. $P < 0.05$ was considered statistically significant. All experiments were performed in triplicate or quadruplicate.

3. Results and discussion

3.1. Characteristics of the PM

The CMC of the PM was measured by evaluating the spectral change of pyrene, which is sensitive to the polarity of the surrounding environment, mixed with an amphiphilic polymeric solution [22,24]. The intensity ratio of the vibronic peak I (I_1) to peak III (I_3) of pyrene decreased from 1.64 for water to 1 for 1-propanol [24]. The change of the I_1/I_3 ratio versus the polymer concentration was, thus, used to obtain the CMC of PM. According to the spectra shown in Fig. S1, the I_1/I_3 ratio decreased sharply at PEO–PPO–PEO polymer concentrations above 0.1%, which was due to the increased hydrophobicity of the pyrene environment in the hydrophobic core region of PPO, indicating the micelle formation of PEO–PPO–PEO block copolymers. Following the first turning point (the defined CMC point at 0.1% PEO–PPO–PEO), a second turning point in the spectrum was observed at a polymer concentration higher than 1% and the I_1/I_3 ratio remained steady afterward (Fig. S1). Therefore, we used a 3% polymer concentration, a concentration above the CMC, for PM preparation in the following experiments to ensure that the micelles of the polymers were present in the formulation. Others have reported that the concentration of polymer micellization determined using either pyrene-based fluorescent probes or surface tension methods is in a similar order of the concentration range near or above the CMC [25,26]. The 3% PM was observed to be spherical with a diameter of approximately 44.66 ± 14.39 nm by TEM and AFM in the tapping mode (Figs. S2A and S2B). The average zeta potential of the

spherical PM was -1.7 ± 0.53 mV, as determined using DLS (Fig. S2C).

3.2. FRET measurements

Two water-insoluble dyes with high energy quantum yields [27], FITC, with a water solubility (S) of 0.09 mg/ml and an octanol–water partition coefficient ($\text{Log } K_{o/w}$) of 5.3, and RhB ($S = 4.4$ mg/ml, $\text{Log } K_{o/w} = 2.1$), were mixed with the 3% PEO–PPO–PEO polymer solution (Fig. S3A). FRET was determined using emission spectroscopy after mixing 180 μM FITC and various concentrations (0–3.6 μM) of RhB with 3% PM. At an excitation wavelength of 490 nm, gradually fading emission intensities of FITC at 520 nm in the PM complexes were detected with the presence of RhB, and the intensity of the RhB emission spectrum detected at 576 nm increased in parallel with the amount of RhB added to the mixture (Fig. 1A). This indicates that FRET between the two dyes occurred in a limited space within the 3% PM. A Stern–Volmer plot was generated using the fluorescence emission intensity of FITC with (F) or without (F_0) RhB [28], and the ratio of the fluorescence emission intensities (F_0/F) of FITC (180 μM) increased linearly with an increasing concentration of RhB (Fig. 1B). The linear slope in the plot with the intercept at 1 on the y-axis shows quenching of FITC, and the linear relationship of this quenching indicates that only one type of dynamic or static quenching effect occurs [23,28], implying close proximity of these two hydrophobic fluorophores in the PM complexes. In addition, the FRET ratio was used to monitor the relative peak transfer between FITC and RhB [29]. The FRET ratio increased from 0.58 to 0.8 in the 3% PM solution when 180 μM FITC was mixed with an increasing concentration of RhB (Fig. 1C). When the concentration of RhB, the FRET acceptor was higher than 0.9 μM , a significantly higher FRET ratio was observed, demonstrating a greater probability of more acceptors capturing the excited energy from the donor fluorophore. A similar result was reported by Gartzia-Rivero et al. [30], who observed a lower FRET ratio when fewer acceptors were present in the reaction. FITC and RhB (at 180 μM and 3 μM concentrations, respectively) were, therefore, mixed with the polymer at various concentrations to examine the status of micellization with respect to the concentration change. Fig. 1D shows that the FRET ratio significantly increased with 0.1% polymer, the identified CMC, following a steep slope on the curve to the point where the polymer concentration reached 1%. An additional increase in the FRET ratio, which plateaued at 0.8, was detected at polymer concentrations higher than 3%, further confirming the efficient energy transfer between the two fluorophores in the intact PM at polymer concentrations passing the second turning point in the pyrene spectrum (Fig. S1). According to another study [26], the solubility of pyrene increases linearly when the polymer concentration is higher than CMC, leading to more pyrene being distributed in the core region. This suggests more FITC and RhB entering the core regions of the PM, increasing the FRET ratio above 0.1% PM. The second turning point, followed by a less marked linear decrease as the PM concentration continued to increase, implied maximal incorporation of FITC and RhB into the formulation. This finding supported by Li et al. [31], shows that 80% of the energy from DiOC₁₈ in the core of micelles was

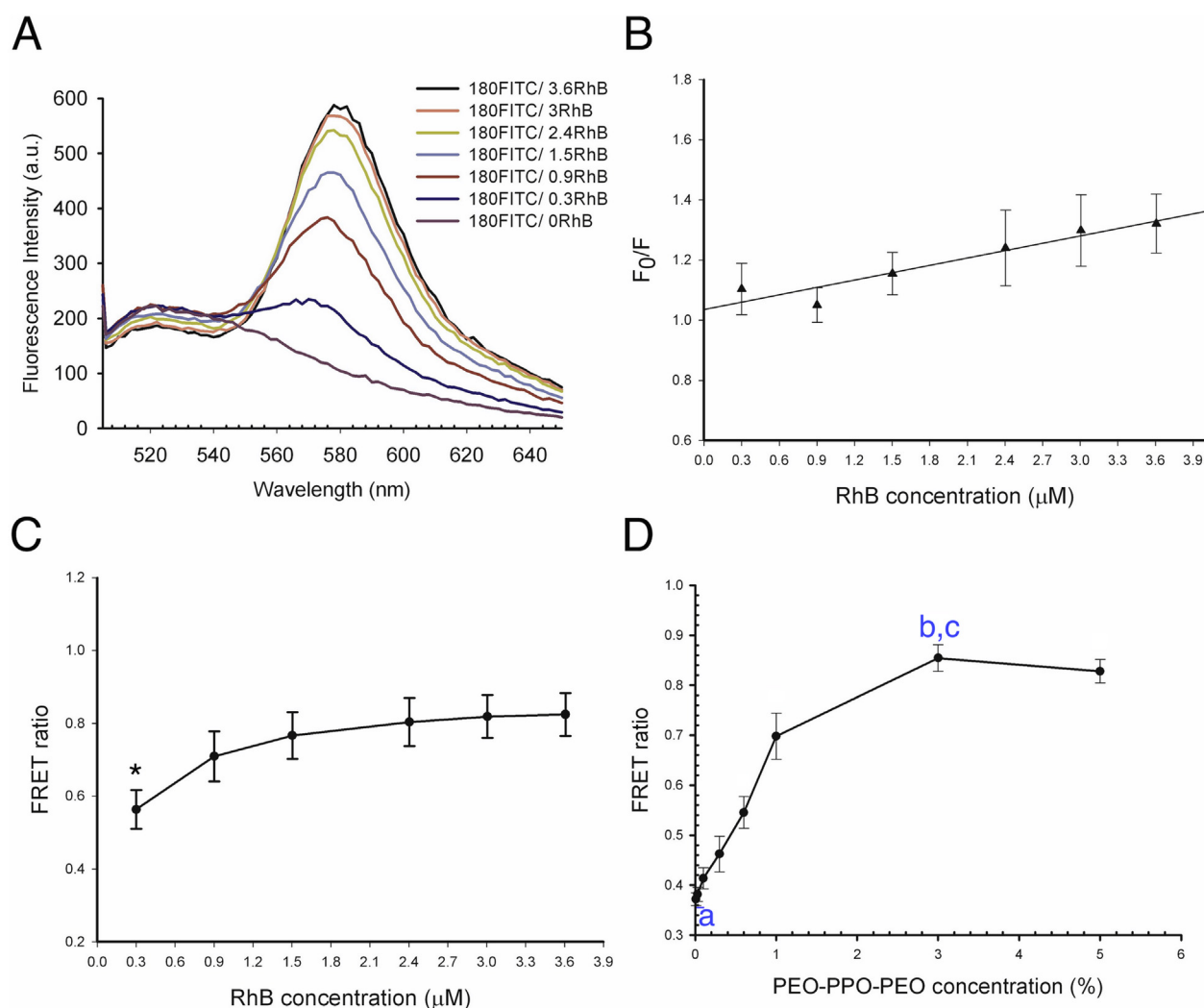


Fig. 1 – Effects of RhB and polymer concentrations on FRET. FRET between FITC at 180 μM and RhB at various concentrations (0–3.6 μM) in PM complexes (A, B, C). (A) The fluorescence intensities of FITC and RhB in PM complexes were measured at an excitation wavelength of 490 nm and with an emission scan from 505 to 650 nm. (B) Stern–Volmer plot illustrating the influence of RhB on FITC in PM complexes. F_0 and F are the fluorescence intensities of FITC (180 μM) in the absence and presence of RhB (0, 0.3, 0.9, 1.5, 2.4, 3, and 3.6 μM), respectively ($n = 3$). (C) The FRET ratio ($I_{576}/(I_{520} + I_{576})$) was calculated from B. (D) FRET ratio of different concentrations of PEO–PPO–PEO polymers mixed with 180 μM FITC and 3 μM RhB ($n = 3$). (*: significant decrease ($P < 0.05$) compared with 1.5, 2.4, 3, and 3.6 μM; a: the polymer concentrations (0.01, 0.03, and 0.1%) were significant decreased ($P < 0.05$) compared with 0.6, 1, 3, and 5%; b: significant increase compared with 0.01, 0.03, 0.1, 0.3, 0.6, and 1% ($P < 0.05$); c: no significant difference between 3 and 5% ($P > 0.05$)).

efficiently transferred to the rhodamine B isothiocyanate conjugated-dendritic cholic acid block copolymers. In addition, Giusti et al. [32] reported that FRET occurred at the micellization concentration of short amphiphilic fluorophores-grafted amphipol polymers. All these results suggest that the changes in the FRET ratio reflect the micellization status of polymers and may be used to determine the stability of PM.

We then evaluated the *in vitro* stability of PM with FITC and RhB, and the results showed that the FRET ratio was reached and maintained at 0.8 within 24 h at room temperature (Fig. S4). This observation implies that FITC and RhB can be stably arranged in close proximity in this PM for at least 24 h and PM can be used as a vehicle for delivery *in vivo*.

3.3. DSC analysis

To evaluate the complexes of FITC and RhB in the PM, a DSC analysis was conducted using 3% PM, FITC, RhB, and 3% PM complexed with FITC and RhB. The thermodynamic data are shown in Fig. S5. At a concentration of 3%, the PM displayed an endothermic peak at its glass transition temperature (50 °C). Likewise, the endothermic peak of RhB, at 164 °C, indicates its melting point. For FITC, the exothermic peak at 287 °C on the DSC diagram signifies crystallization. However, when FITC and RhB were complexed with 3% PM, only an endothermic peak at 50 °C was observed in the DSC diagram, whereas the characteristic peaks of FITC and RhB were absent. When heated to 400 °C, the complex disintegrated and was

accompanied by an exothermic reaction. A previous study [33] reported that all of the characteristic peaks of a sample were missing in the DSC pattern when the sample was complexed with PM. This suggests that FITC and RhB were complexed with PM. In addition, TEM data showed that the sizes of the PM complexes with FRET pairs decreased to 17.01 ± 5.32 nm (Fig. S6A). Han et al. [34] found that both the core and shell sizes of PM decreased in the presence of hydrophobic drugs. They suggested that the volume fraction of polymers in the core region might depend on drug molecules substituted in the PM structure.

3.4. Confocal imaging of the PM complex

Confocal imaging was used to monitor the distribution of FRET pairs mixed with 3% PM *in vitro*. At an excitation wavelength of 488 nm, which excited only FITC, FRET was observed in PM with free FITC and RhB, as evidenced by red fluorescence signals emitted from the RhB channel (Fig. 2, upper three images). This further confirms proximal colocalization of the two hydrophobic fluorophores in the limited space provided by PM. To delineate the spatial proximity of the hydrophobic molecules and the polymer, 3% FITC-P was mixed with RhB (Fig. S3B). The results showed that, within the same particle, the fluorescence signals emitted from both FITC and

RhB were detected at nearly the same position (Fig. 2, middle three images). This suggests that the free hydrophobic fluorophore, RhB, may be distributed to the core of 3% PM at nanoscale sizes in such a juxtaposition that allows efficient FRET to occur. A similar FRET approach was applied to evaluate the stability of PM formulated with 3% FITC-P and RhB-labeled DNA (RhB-DNA) (Fig. S3C), which were determined have a size of 41.24 ± 13.69 nm through TEM (Fig. S6B). FITC and RhB fluorescence signals were observed to be colocalized in the PM area (Fig. 2, lower three images). Itaka et al. [35] reported a similar result with poly(ethylene glycol)-poly(L-lysine) PM complexes, observing FRET between FRET pairs conjugated on the same DNA molecules condensed with PM. The fluorescence signals shown on our confocal microscope images are somewhat larger compared with the respective TEM image; this result is attributable to diffraction that occurs when the particle size is smaller than the wavelength of radiation [36].

3.5. *In vitro* corneal permeation of FRET pairs complexed with PM

The permeation of FRET pairs (FITC and RhB) complexed with 3% PM through the cornea was evaluated using Franz cells. At an excitation wavelength of 490 nm, which excited FITC, the

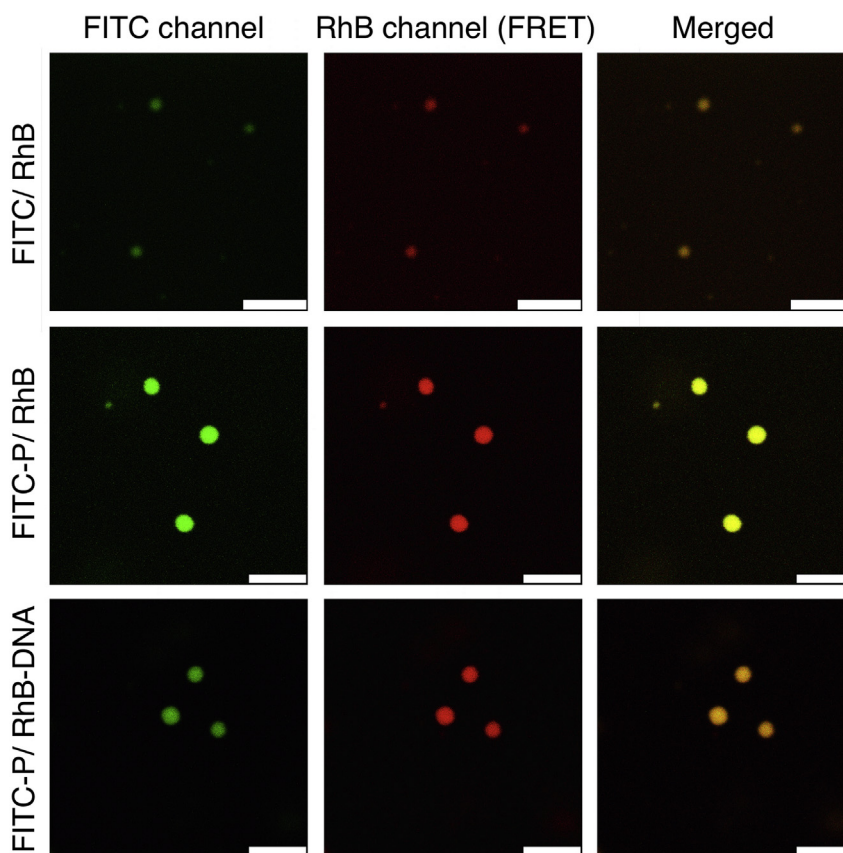


Fig. 2 – Confocal micrographs of PM complexes confocal microscopy images of PEO–PPO–PEO PM with FITC and RhB, FITC-labeled PEO–PPO–PEO polymeric micelles (FITC-P) with RhB, and FITC-P with RhB-labeled plasmids (RhB-DNA) at an excitation wavelength of 488 nm. The emission data were collected between 500 and 550 nm for FITC channel and 565 and 650 nm for RhB channel, respectively. Green and red denote FITC and RhB signals, respectively. Yellow represents fluorescence co-localization two signals in the merged panel. Scale bar = 5 μ m.

occurrence of FRET was detected by measuring emission at a wavelength of 576 nm from RhB (Fig. 3A). During the 4-h permeation period, a gradual increase in the fluorescence intensity at 576 nm was observed. The FRET ratio significantly increased from 0.48 to 0.8 after 2 h (Fig. 3B), suggesting the presence of the PM complexed with FRET pairs on the receiver. According to Fig. 1, the FRET ratio was influenced by both the RhB and polymer concentrations. In addition, the cornea transport of dexamethasone carriers composed of poloxamer 407, which is a PEO–PPO–PEO polymer, was evaluated on cornea transport [37]. Approximately 30 min after incubation, these polymers were found to be able to penetrate the rabbit cornea. Here, we detected the presence of PEO–PPO–PEO polymers in the mouse corneal endothelium at 1.5 h after permeation (Fig. S7). Therefore, the results indicated that FRET pairs complexed with PM could permeate the cornea 2 h after administration.

3.6. In vivo distribution of FITC and RhB complexes with PM in the cornea

To confirm the stability of PM carrying small molecules or macromolecules to ocular tissues, we used confocal microscopy to observe the intracorneal distribution of FRET pair dyes with 3% PM. One hour after administering 10 μ l of eye drops with PM and FRET pair dyes on the cornea, PM with both FRET pair dyes were dispersed in the cytoplasm, and surrounded and entered the nuclei of cells in the corneal epithelium (Fig. 4A, Fig. S8). Compared to the images of the PM complexes with FITC group, FRET was detected in the cornea treated with PM and free FRET pair dyes (FITC and RhB). Furthermore, colocalization of fluorescence in the cytoplasm and cell nucleus of the corneal epithelium was confirmed in tissues administered RhB or RhB–DNA complexed with FITC-P (Fig. 4A). These results support the concept that the two free fluorophores, DNA-conjugated, or

polymer-conjugated, may stably locate in proximity within the PM with sufficient integrity for energy transfer after delivery to the cornea. A rabbit monoclonal anti-PEG IgG with specificity for 16 oxyethylene repeat units [38] was used to immunohistochemically detect and confirm the presence of the PEO ends of PEO–PPO–PEO and FITC-P in the corneal tissues. Positive signals for the anti-PEG IgG (Fig. 4B) supported the delivery of PEO–PPO–PEO polymers to corneal epithelial layers and their distribution in the cytoplasm and the surface of the nucleus 1 h after administration. The stability of PM with FRET pairs or DNA delivered into the corneal epithelium may be attributed to the pegylation of the PEO shell of the PM. Previous studies have suggested that the pegylation of carriers may overcome corneal barriers to aid in ocular delivery [39,40]. Studies has also shown that the pegylation of solid nanoparticles, such as PEG-coated poly- ϵ -caprolactone nanocapsules, facilitates *in vitro* corneal epithelium delivery 1 h after incubation [39,40]. According to the finding that fluorophore-loaded PEG-coated nanocapsules has been distributed inside the corneal epithelium cells, rather than in the intercellular space, the delivery of pegylated carriers was considered to occur via a transcellular pathway [40,41]. Similar results have been reported for pegylated carriers delivering genes [17,42]. Pegylated PEI nanoparticles with DNA appeared as discrete particles accumulated in a perinuclear region or as particles moving toward the nucleus in BHK-21 cells [42]. Arranja et al. [41] reported that PEO–PPO–PEO polymers, the carriers used in our study, were internalized and dispersed in the cytoplasm and around or inside the nuclei of cervical cancer HeLa and glioblastoma U87 cells and suggested a caveolae-mediated endocytosis for the transcellular transport of PEO–PPO–PEO carriers. We previously reported a decrease in the expression level of genes delivered by this PM in mice pretreated with RGD peptide, an endocytotic inhibitor with a critical integrin binding motif [43], also supporting the endocytosis entry

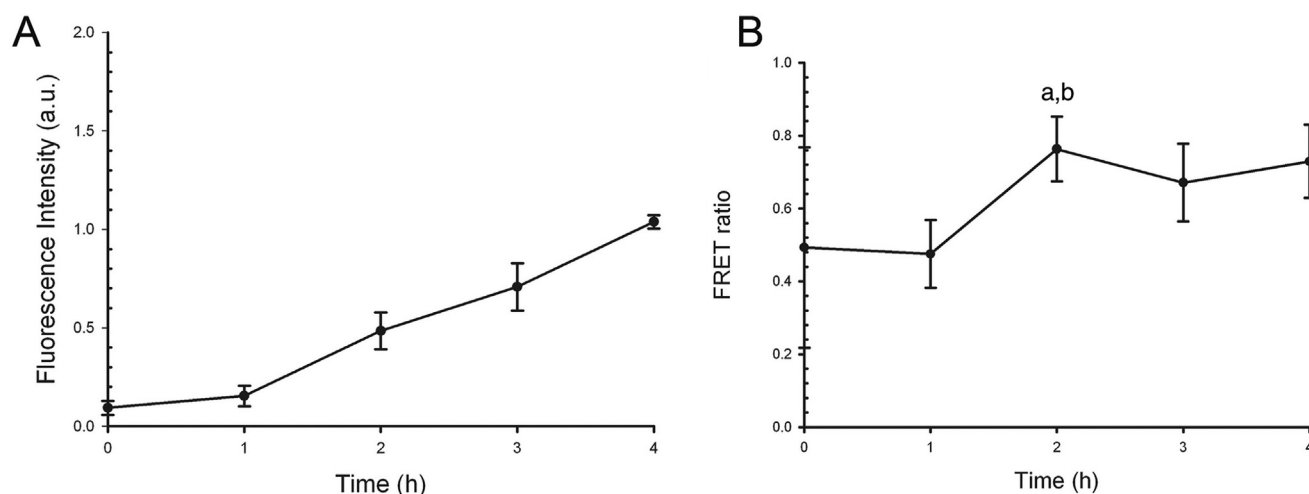


Fig. 3 – Stability of FRET pair complexes with PM after permeation *in vitro* (A) Cornea permeation profiles of FRET pairs (FITC and RhB) complexed with 3% PEO–PPO–PEO PM on the cornea (each value represents the mean \pm S.D. of $n = 4$). The fluorescence intensities of RhB in PM complexes were measured at excitation and emission wavelength of 490 nm and 576 nm, respectively. (B) The FRET ratio ($I_{576}/(I_{520} + I_{576})$) of 180 μ M FITC and 3 μ M RhB complexed with PM was calculated from (A). a: significant increase ($P < 0.05$) compared with 0 and 1 h; b: no significant difference among 2, 3, and 4 h ($P > 0.05$).

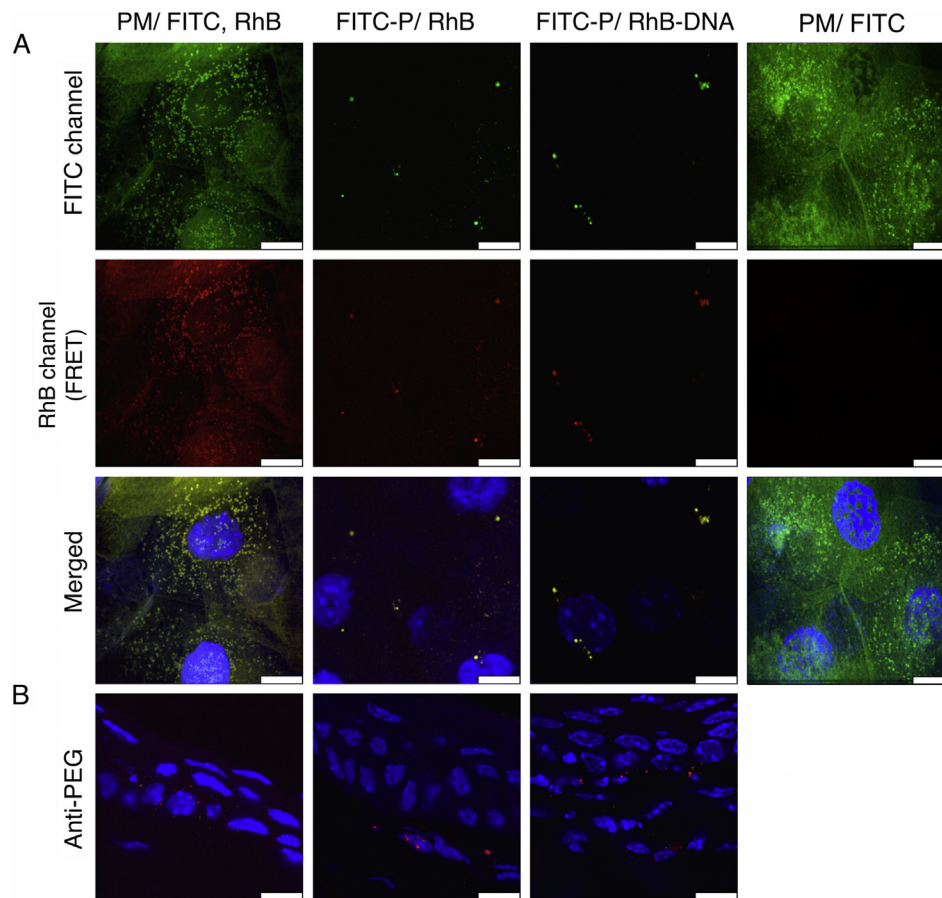


Fig. 4 – *In vivo* distribution of PM complexes in the cornea Intracellular distribution of 3% PM complexes with DAPI nuclear staining (blue) of the cornea 1 h after a topically delivered dose (10 μ l) was administered. PM with FITC and RhB, FITC-P with RhB, and FITC-P with RhB–DNA compared with PM complexes with FITC. (A) Confocal images of the freshly mounted cornea at an excitation wavelength of 488 nm. The merged images were overlaid with emission images of FITC and RhB. (B) Confocal images of anti-PEG Immunostaining (red) of cross-sections of the cornea. Scale bar = 10 μ m.

mechanism of the PM [17]. PEO–PPO–PEO has been approved by the United States Food and Drug Administration for the use in ophthalmic pharmaceuticals [14], and in our previous study [16], we did not find any cellular inflammatory response, judged by the absence of polymorphonuclear or round cell infiltration with hematoxylin–eosin staining of the eyes after six doses for 2 days. We also detected the presence of PEO–PPO–PEO polymers in the endothelium of mouse corneal at 1.5 h after permeation (Fig. S7). However, due to the natural aqueous humor dilution effect and drainage through the trabecular meshwork into Schlemm's canal, whether PEO–PPO–PEO PM remain intact to reach an aqueous humor area or are eliminated/or metabolized in the circulatory system requires further study.

4. Conclusion

The stability of insoluble fluorophores or plasmid DNA with PEO–PPO–PEO polymers was monitored through fluorescence-based methods *in vitro* and *in vivo*. Quenching and FRET were analyzed for mixtures of FITC and RhB with 3%

PM. The complexes of FRET pairs with PM were also detected through a DSC measurement. The change of the FRET ratio during the formation of PM provides a sensitive criterion to monitor the integrity of PM during delivery. After 2 h, we observed the penetration of PM complexes with FRET pairs through the cornea by measuring the FRET ratio *in vitro*. The insoluble fluorophores or hydrophilic plasmids DNA with PM were found to be colocalized *in vitro* and in corneal tissues, confirming the feasibility and stability of PM as carriers for therapeutic molecules.

Funding

This work was supported by grants from the Ministry of Science and Technology, Taiwan [MOST 104-2320-B-038-014-MY2 and NSC 101-2320-B-038-008-MY3].

Conflicts of interest

The authors declare no competing financial interest.

Appendix A. Supplementary data

Supplementary data related to this article can be found at <https://doi.org/10.1016/j.jfda.2017.09.002>.

REFERENCES

- [1] Al Khateb K, Ozhmukhametova EK, Mussin MN, Seilkhanov SK, Rakhypbekov TK, Lau WM, et al. In situ gelling systems based on Pluronic F127/Pluronic F68 formulations for ocular drug delivery. *Int J Pharm* 2016;502:70–9.
- [2] Mohamed EA, Abu Hashim II, Yusif RM, Suddek GM, Shaaban AAA, Badria FAE. Enhanced in vitro cytotoxicity and anti-tumor activity of vorinostat-loaded pluronic micelles with prolonged release and reduced hepatic and renal toxicities. *Eur J Pharm Sci* 2017;96:232–42.
- [3] Chen CL, Chang SF, Lee D, Yang LY, Lee YH, Hsu CY, et al. Bioavailability effect of methylprednisolone by polymeric micelles. *Pharm Res* 2008;25:39–47.
- [4] Gao ZG, Fain HD, Rapoport N. Controlled and targeted tumor chemotherapy by micellar-encapsulated drug and ultrasound. *J Control Rel* 2005;102:203–22.
- [5] Chang SF, Chang HY, Tong YC, Chen SH, Hsaio FC, Lu SC, et al. Nonionic polymeric micelles for oral gene delivery in vivo. *Hum Gene Ther* 2004;15:481–93.
- [6] Wenzel JG, Balaji KS, Koushik K, Navarre C, Duran SH, Rahe CH, et al. Pluronic F127 gel formulations of deslorelin and GnRH reduce drug degradation and sustain drug release and effect in cattle. *J Control Rel* 2002;85:51–9.
- [7] Liaw J, Lin Y-C. Evaluation of poly(ethylene oxide)–poly(propylene oxide)–poly(ethylene oxide) (PEO–PPO–PEO) gels as a release vehicle for percutaneous fentanyl. *J Control Rel* 2000;68:273–82.
- [8] Chao YC, Chang SF, Lu SC, Hwang TC, Hsieh WH, Liaw J. Ethanol enhanced in vivo gene delivery with non-ionic polymeric micelles inhalation. *J Control Rel* 2007;118:105–17.
- [9] Alai MS, Lin WJ, Pingale SS. Application of polymeric nanoparticles and micelles in insulin oral delivery. *J Food Drug Anal* 2015;23:351–8.
- [10] Ma Y, Pandzic E, Nicovich PR, Yamamoto Y, Kwiatek J, Pagon SV, et al. An intermolecular FRET sensor detects the dynamics of T cell receptor clustering. *Nat Commun* 2017;8:15100.
- [11] Basak D, Ghosh S. pH-regulated controlled swelling and sustained release from the core functionalized amphiphilic block copolymer micelle. *ACS Macro Lett* 2013;2:799–804.
- [12] Stevens GA, White RA, Flaxman SR, Price H, Jonas JB, Keeffe J, et al. Global prevalence of vision impairment and blindness. *Ophthalmology* 2013;120:2377–84.
- [13] Di Tommaso C, Bourges J-L, Valamanesh F, Trubitsyn G, Torriglia A, Jeanny J-C, et al. Novel micelle carriers for cyclosporin A topical ocular delivery: in vivo cornea penetration, ocular distribution and efficacy studies. *Eur J Pharm Biopharm* 2012;81:257–64.
- [14] Pepić I, Jalsenjak N, Jalsenjak I. Micellar solutions of triblock copolymer surfactants with pilocarpine. *Int J Pharm* 2004;272:57–64.
- [15] Rowe-Rendleman CL, Durazo SA, Kompella UB, Rittenhouse KD, Di Polo A, Weiner AL, et al. Delivery to the back of the eye: from bench to bedside. *Investig Ophthalmol Vis Sci* 2014;55:2714–30.
- [16] Liaw J, Chang SF, Hsiao FC. In vivo gene delivery into ocular tissues by eye drops of poly(ethylene oxide)-poly(propylene oxide)-poly(ethylene oxide) (PEO-PPO-PEO) polymeric micelles. *Gene Ther* 2001;8:999–1004.
- [17] Tong YC, Chang SF, Liu CY, Kao WW, Huang CH, Liaw J. Eye drop delivery of nano-polymeric micelle formulated genes with cornea-specific promoters. *J Gene Med* 2007;9:956–66.
- [18] Tong YC, Chang SF, Kao WW, Liu CY, Liaw J. Polymeric micelle gene delivery of bcl-xL via eye drop reduced corneal apoptosis following epithelial debridement. *J Control Rel* 2010;147:76–83.
- [19] Maysinger D, Lovric J, Eisenberg A, Savic R. Fate of micelles and quantum dots in cells. *Eur J Pharm Biopharm* 2007;65:270–81.
- [20] Savic R, Azzam T, Eisenberg A, Maysinger D. Assessment of the integrity of poly(caprolactone)-b-poly(ethylene oxide) micelles under biological conditions: a fluorogenic-based approach. *Langmuir* 2006;22:3570–8.
- [21] Tavitou E, Barry BW. Enhancement in drug delivery. Boca Raton: CRC Press; 2007.
- [22] Liaw J, Aoyagi T, Kataoka K, Sakurai Y, Okano T. Permeation of PEO-PBLA-FITC polymeric micelles in aortic endothelial cells. *Pharm Res* 1999;16:213–20.
- [23] Lakowicz JR, Weber G. Quenching of fluorescence by oxygen. A probe for structural fluctuations in macromolecules. *Biochemistry* 1973;12:4161–70.
- [24] Kalyanasundaram K, Thomas JK. Environmental effects on vibronic band intensities in pyrene monomer fluorescence and their application in studies of micellar systems. *J Am Chem Soc* 1977;99:2039–44.
- [25] Sezgin Z, Yuksel N, Baykara T. Preparation and characterization of polymeric micelles for solubilization of poorly soluble anticancer drugs. *Eur J Pharm Biopharm* 2006;64:261–8.
- [26] Alexandridis P, Nivaggioli T, Hatton TA. Temperature effects on structural properties of pluronic P104 and F108 PEO-PPO-PEO block copolymer solutions. *Langmuir* 1995;11:1468–76.
- [27] McClatchey KD. *Clinical laboratory medicine*. 2nd ed. Philadelphia: Lippincott Williams & Wilkins; 2002.
- [28] Pham W, Choi Y, Weissleder R, Tung CH. Developing a peptide-based near-infrared molecular probe for protease sensing. *Bioconjugate Chem* 2004;15:1403–7.
- [29] Lu J, Owen SC, Shoichet MS. Stability of self-assembled polymeric micelles in serum. *Macromol* 2011;44:6002–8.
- [30] Gartzia-Rivero L, Cerdán L, Bañuelos J, Enciso E, López Arbeloa Í, Costela Á, et al. Förster resonance energy transfer and laser efficiency in colloidal suspensions of dye-doped nanoparticles: concentration effects. *J Phys Chem C* 2014;118:13107–17.
- [31] Li Y, Xiao W, Xiao K, Berti L, Luo J, Tseng HP, et al. Well-defined, reversible boronate crosslinked nanocarriers for targeted drug delivery in response to acidic pH values and cis-diols. *Angew Chem Int Ed Engl* 2012;51:2864–9.
- [32] Giusti F, Popot JL, Tribet C. Well-defined critical association concentration and rapid adsorption at the air/water interface of a short amphiphilic polymer, amphipol A8-35: a study by Förster resonance energy transfer and dynamic surface tension measurements. *Langmuir* 2012;28:10372–80.
- [33] Saxena V, Hussain MD. Formulation and in vitro evaluation of 17-allylamino-17-demethoxygeldanamycin (17-AAG) loaded polymeric mixed micelles for glioblastoma multiforme. *Colloids Surf B Biointerfaces* 2013;112:350–5.
- [34] Han Y, Zhang Z, Smith GS, Do C. Effect of nucleoside analogue antimetabolites on the structure of PEO–PPO–PEO micelles investigated by SANS. *Phys Chem Chem Phys* 2017;19:15686–92.
- [35] Itaka K, Yamauchi K, Harada A, Nakamura K, Kawaguchi H, Kataoka K. Polyion complex micelles from plasmid DNA and

- poly(ethylene glycol)–poly(l-lysine) block copolymer as serum-tolerable polyplex system: physicochemical properties of micelles relevant to gene transfection efficiency. *Biomaterials* 2003;24:4495–506.
- [36] Minin I, Minin O. *Diffractive optics and nanophotonics: resolution below the diffraction limit*. Springer International Publishing; 2016.
- [37] Gan L, Han S, Shen J, Zhu J, Zhu C, Zhang X, et al. Self-assembled liquid crystalline nanoparticles as a novel ophthalmic delivery system for dexamethasone: improving preocular retention and ocular bioavailability. *Int J Pharm* 2010;396:179–87.
- [38] Veronese FM. *PEGylated protein drugs: basic science and clinical applications*. Basel; Boston: Birkhäuser; 2009.
- [39] Mun EA, Morrison PW, Williams AC, Khutoryanskiy VV. On the barrier properties of the cornea: a microscopy study of the penetration of fluorescently labeled nanoparticles, polymers, and sodium fluorescein. *Mol Pharm* 2014;11:3556–64.
- [40] De Campos A. The effect of a PEG versus a chitosan coating on the interaction of drug colloidal carriers with the ocular mucosa. *Eur J Pharm Sci* 2003;20:73–81.
- [41] Arranja A, Denkova AG, Morawska K, Waton G, van Vlierberghe S, Dubruel P, et al. Interactions of Pluronic nanocarriers with 2D and 3D cell cultures: effects of PEO block length and aggregation state. *J Control Rel* 2016;224:126–35.
- [42] Mishra S, Webster P, Davis ME. PEGylation significantly affects cellular uptake and intracellular trafficking of non-viral gene delivery particles. *Eur J Cell Biol* 2004;83:97–111.
- [43] Scarborough RM, Rose JW, Naughton MA, Phillips DR, Nannizzi L, Arfsten A, et al. Characterization of the integrin specificities of disintegrins isolated from American pit viper venoms. *J Biol Chem* 1993;268:1058–65.